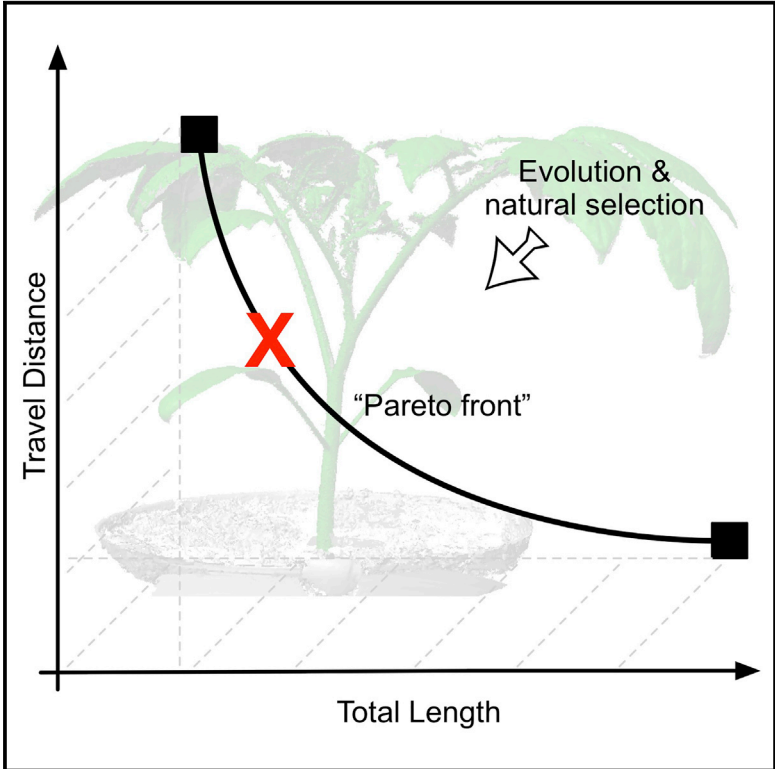


Cell Systems

High-Resolution Laser Scanning Reveals Plant Architectures that Reflect Universal Network Design Principles

Graphical Abstract



Authors

Adam Conn, Ullas V. Pedmale, Joanne Chory, Saket Navlakha

Correspondence

navlakha@salk.edu

In Brief

Conn et al. analyzed 505 three-dimensional plant shoot architectures and discovered that plant architectures achieve an optimal trade-off between two common network design measures: minimizing construction costs and minimizing transport distances. This result highlights a principle of plant form shared by many engineered and biological transport networks.

Highlights

- We scanned 505 3D plant architectures across species, conditions, and time points
- Plant architectures are Pareto optimal in a network cost versus performance trade-off
- The location on the Pareto front is indicative of a plant's species or condition



High-Resolution Laser Scanning Reveals Plant Architectures that Reflect Universal Network Design Principles

Adam Conn,¹ Ullas V. Pedmale,^{2,3} Joanne Chory,² and Saket Navlakha^{1,4,*}

¹Integrative Biology Laboratory, The Salk Institute for Biological Studies, La Jolla, CA, USA

²Howard Hughes Medical Institute and Plant Biology Laboratory, The Salk Institute for Biological Studies, La Jolla, CA, USA

³Present address: Cold Spring Harbor Laboratory, Cold Spring Harbor, New York, NY, USA

⁴Lead Contact

*Correspondence: navlakha@salk.edu

<http://dx.doi.org/10.1016/j.cels.2017.06.017>

SUMMARY

Transport networks serve critical functions in biological and engineered systems, and yet their design requires trade-offs between competing objectives. Due to their sessile lifestyle, plants need to optimize their architecture to efficiently acquire and distribute resources while also minimizing costs in building infrastructure. To understand how plants resolve this design trade-off, we used high-precision three-dimensional laser scanning to map the architectures of tomato, tobacco, or sorghum plants grown in several environmental conditions and through multiple developmental time points, scanning in total 505 architectures from 37 plants. Using a graph-theoretic algorithm that we developed to evaluate design strategies, we find that plant architectures lie along the Pareto front between two simple length-based objectives—minimizing total branch length and minimizing nutrient transport distance—thereby conferring a selective fitness advantage for plant transport processes. The location along the Pareto front can distinguish among species and conditions, suggesting that during evolution, natural selection may employ common network design principles despite different optimization trade-offs.

INTRODUCTION

Transport networks, which are ubiquitous in engineering and biology, perform many essential functions. In engineering, subway systems, roads, and the power grid all serve to collect and distribute entities (people, cars, energy) from one location to another (Newman, 2010). In biology, transport networks are used by ants to organize foraging trails (Cabanes et al., 2014), by slime molds to discover and exploit food sources (Tero et al., 2010), and by dendrites and axons to collect and transmit information within neuronal circuits (Budd et al., 2010; Cuntz et al., 2010).

The design of transport networks faces fundamental trade-offs that affect their structure and function. For example, building

and maintaining networks can be costly, as measured by the amount of material or labor required for construction; further, physically moving entities through a network often requires limiting resources, such as power or energy. These costs, however, must be borne in order to design a useful system that provides efficient transport performance.

Here, we seek to understand whether this tension between cost and performance helps dictate plant architecture, and if so, how plants resolve this tension. The architecture of a plant is used to acquire resources from the environment and to distribute nutrients among different organs (Rolland et al., 2002; Peel, 2013). We view the architecture of a plant as a 3D geometric network. Nodes in this network correspond to the base of the stem, the leaves, or branch points, each physically embedded in 3D space. Edges represent conductive elements, such as the stem, hypocotyl, or petioles, connecting two nodes (Godin, 2000; Prusinkiewicz and Runions, 2012) (Figure S1A). The network should contain a path from each leaf to the base of the stem where the root system lies in order to provide efficient routes for nutrient transport (Roitsch, 1999; Williams et al., 2000).

Prior work has discovered many mathematical principles of plant structure, including phyllotaxis (Jean, 2009), planar bifurcation patterning (Kim et al., 2012), fractal self-similarity of branching (West et al., 1999; Godin and Ferraro, 2010; Mandelbrot and Novak, 2004), and allometries in various plant parts (Niklas, 2004; Price et al., 2009; Price and Weitz, 2012; Smith et al., 2014). These properties are captured by several models of plant architectures, including Lindenmayer systems (Prusinkiewicz and Lindenmayer, 1996; Allen et al., 2005; Ochoa, 1998; Boudon et al., 2012) and metabolic scaling models (Banavar et al., 2002; Price et al., 2010; Sperry et al., 2012). Functional-structural models (Vos et al., 2010; Fourcaud et al., 2008; Guo et al., 2011; Simini et al., 2010) have also been used to simulate how different physiological factors, such as organ topology, leaf geometry, and carbon allocation, influence plant structure and function. These and other studies (Corson, 2010) provide useful constraints that model realistic plant shapes. Here, we build upon these works to analyze network design trade-offs, where the goal is to create an efficient network that connects a base point to leaf points in 3D space. We analyze “skeletonized” versions of plant architectures, evaluating them based only on length measurements to test a network cost-performance trade-off without requiring a model with many parameters.

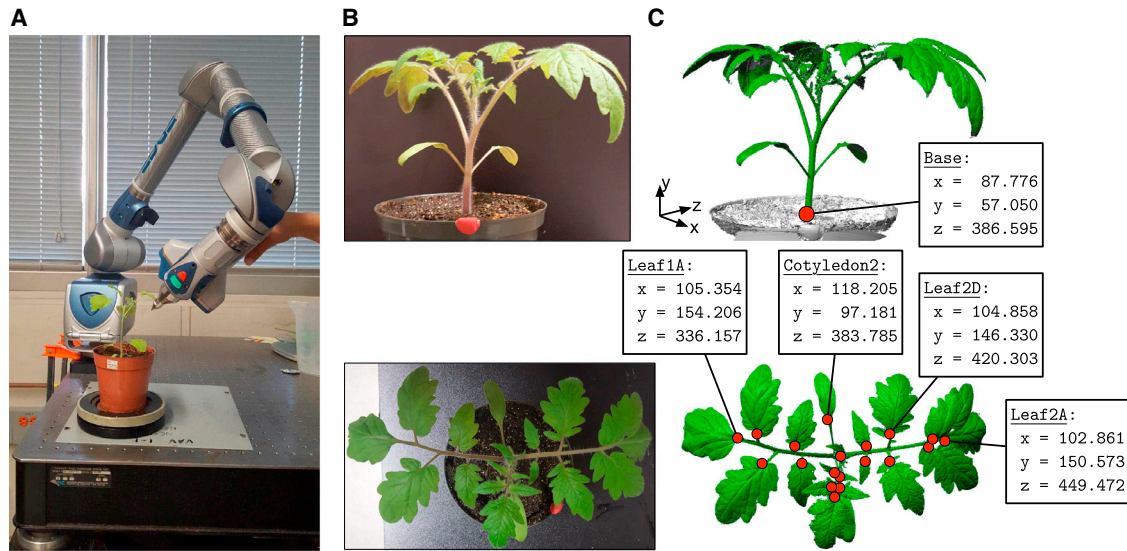


Figure 1. High-Resolution 3D Scanning of Plant Architecture

(A) A 3D laser scanner with rotating arm fixed to an anti-vibration table.

(B) Image of a tomato plant grown in ambient conditions on scanning day 20, with side and top views.

(C) Corresponding 3D scan of the plant with 940,381 cloud points, excluding the soil and pot. The (x, y, z) coordinates of the base and a few sample leaves are shown. "Leaf2D" corresponds to the fourth leaflet of the second leaf. Related to [Figures S1](#) and [S3](#).

Lengths by themselves do not capture all trade-offs made by plant architectures (see [Discussion](#)); however, they are related to several known biological factors that affect plant function, including hydraulic resistance and construction costs.

Overall, we offer the following contributions:

1. Collection of an extensive dataset of 505 above-ground plant architectures, spanning 3 species, 3–5 developmental conditions for the same species, and 20 developmental time points for the same plant, each captured using high-resolution 3D laser scanning.
2. Development of a graph-theoretic algorithm to evaluate network design trade-offs, and analysis showing that most plant architectures are Pareto optimal in two simple cost and performance measures.
3. Evidence that the location of a plant on the Pareto front is indicative of different trade-offs made in different species or growth conditions.

We conclude by describing how the trade-offs faced by plant architectures are also faced by other branching structures, including dendrites, axons, and vasculature, suggesting the broad importance of these network design principles in biology.

RESULTS

3D Scanning of Plant Architectures

We used 3D scanning technology to generate high-resolution measurements of plant architectures ([Figure 1A](#)). The scanner is non-contact, allowing for multiple scans of the same plant over time without perturbing the plant. Overall, we digitized 505 different plant architectures, spanning 3 species (tomato, tobacco, sorghum), 3–5 environmental growth conditions (ambient

light, shade, high heat, high light, drought), and through approximately 20 days of growth ([STAR Methods](#)).

From each plant scan, we extracted (x, y, z) points representing the location of the base and leaves of the plant in 3D space ([Figures 1B](#) and [1C](#)). These points were used as input to the graph-theoretic analysis described below.

A Graph-Theoretic Framework for Analyzing Plant Architectures

We developed a framework to quantify the trade-off between cost and performance of plant architectures using the theory of Pareto optimality. This theory is often used in economics and engineering to find satisfiable solutions that best trade off multiple, competing objectives ([Farnsworth and Niklas, 1995](#); [Kennedy, 2010](#)).

As input, we are given a set of points, $P = (p_0, p_1, p_2, \dots, p_n)$ in 3D Euclidean space ([Figure 2A](#)). The point p_0 corresponds to the base of the plant and the remaining n points correspond to the locations of the plant's leaves and leaflets. The goal is to find a set of undirected edges or branches \mathcal{B} such that there exists exactly one path from p_0 to each leaf. Water and nutrients may flow in either direction—from a leaf or toward a leaf—and thus we model our edges as undirected. A path is defined as a sequence of edges, starting from the base node p_0 , passing through zero or more branch points, and terminating at a leaf node. All edges are treated as one-dimensional (length only). Non-input points, called Steiner nodes, may also be added to the network as branch points to reduce the length of the connecting architecture ([Smith, 1992](#)).

Performance and cost are two metrics often used to evaluate the design of transport networks ([Tero et al., 2010](#); [Pestana et al., 2004](#)). We measure performance, called travel distance, as the sum of the distances along the branches from the base to

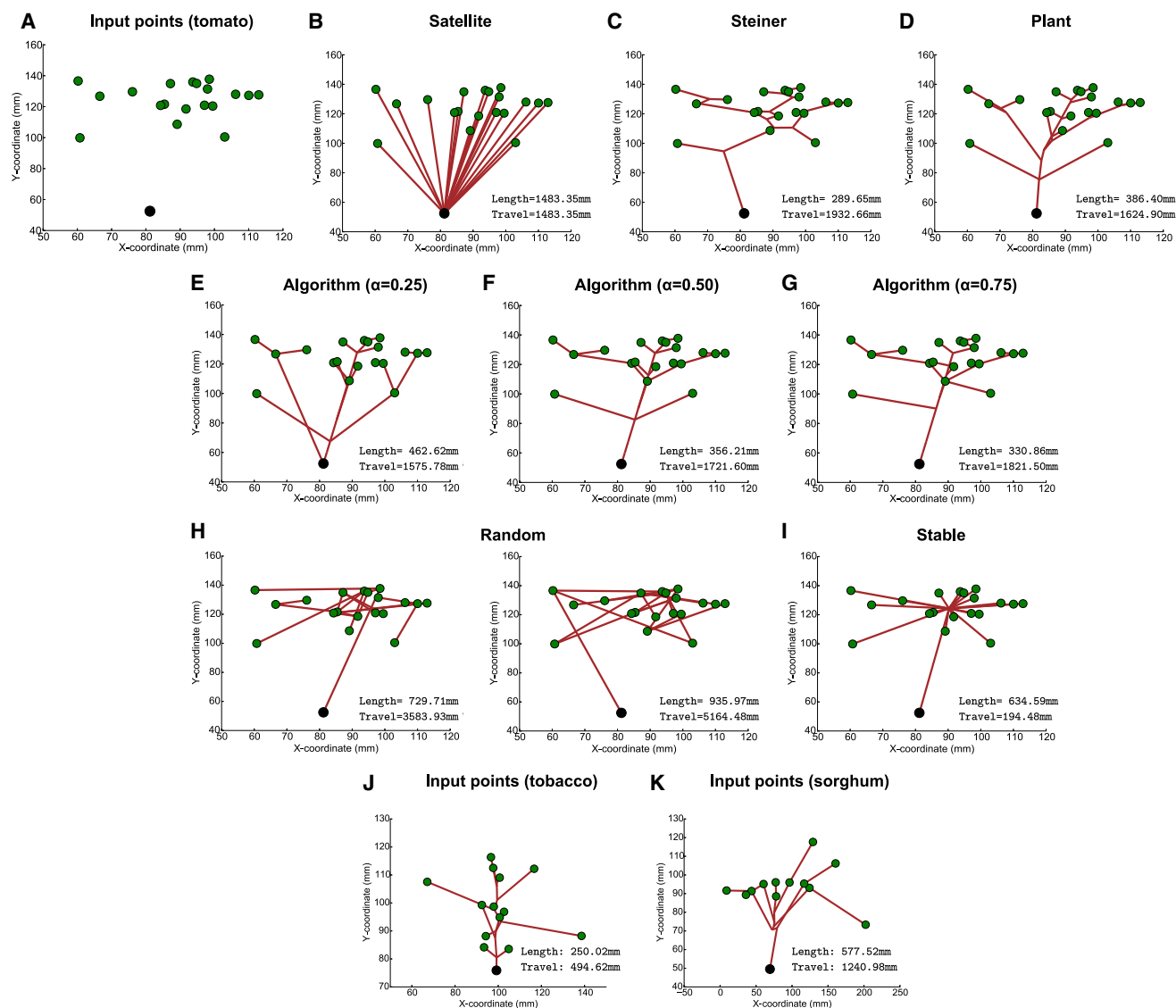


Figure 2. Graph-Theoretic Framework and Example Architectures

(A) Example input points derived from a 3D scan of a tomato plant on scanning day 20 grown in ambient conditions. The points represent the locations of the base of the stem (black point) and leaves/leaflets (green points).

(B) The Satellite tree, which optimally minimizes travel distance.

(C) The Steiner tree, which optimally minimizes total branch length.

(D) The actual plant architecture connecting the input points through branch points.

(E–G) Example trees derived using our algorithm for different values of the trade-off parameter, α .

(H) Random spanning trees.

(I) Stable tree.

(J) Example input points and architecture for a tobacco plant.

(K) Example input points and architecture for a sorghum plant.

In each panel, the values of the two objective functions are shown. All analysis is done in 3D, but points here are embedded in 2D for visualization.

Related to [Algorithm S1](#) and [Table S2](#).

each leaf. We measure cost, called total length, as the sum of all the branch lengths. While general, these objectives can be cast in terms of known biological currencies. Travel distance is related to many known performance measures of plant architectures, including hydraulic resistance and metabolic energy, which is required to transport sugars, nutrients, and water between the leaves and the root system ([McCulloh et al., 2003](#);

[Price et al., 2007, 2010](#); [Peel, 2013](#); [Shinozaki et al., 1964](#)); travel distance can also measure time delays in wound signaling responses, which affect healing rates ([Leon et al., 2001](#)). Total length is a measure of the total investment of resources (carbon, nutrients) required to build the architecture ([Bloom et al., 1985](#)); minimizing total length can also aid in weight and posture control ([Domec et al., 2008](#); [Savage et al., 2010](#)). Thus, these two

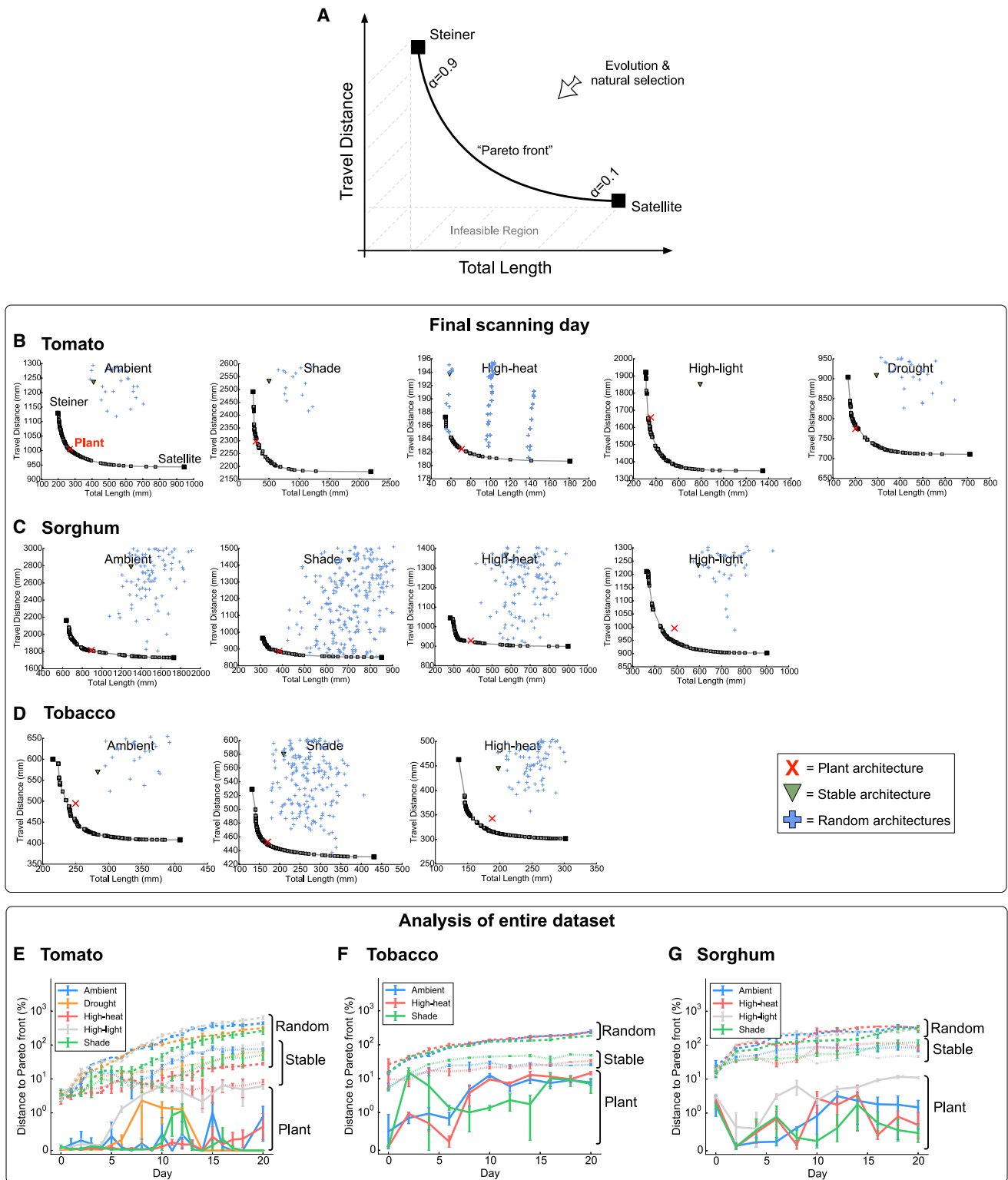


Figure 3. Plant Architectures Are Pareto Optimal

(A) Mock trade-off diagram of the Pareto front between the individual optimals (Steiner and Satellite) of the two objectives. Regions to the left of Steiner on the x axis and below Satellite on the y axis are by definition infeasible. Evolution and natural selection should push architectures toward the Pareto front.

(B–D) Actual trade-off diagrams for tomato, tobacco, and sorghum plants for each condition on the final scanning day. The red cross in each diagram denotes the location of the plant. The two black squares denote the Steiner and Satellite optimals. The gray squares correspond to architectures generated by our algorithm

(legend continued on next page)

measures are relevant to biological cues that affect plant function and growth, although they by no means capture all possible trade-offs made.

These two metrics are formally defined below:

$$\text{Travel}(\mathcal{P}, \mathcal{B}) := \sum_{i=1}^n \text{dist}_{\mathcal{B}}(\rho_0, \rho_i) \quad (\text{Equation 1})$$

$$\text{Length}(\mathcal{P}, \mathcal{B}) := \sum_j |\mathcal{B}_j| \quad (\text{Equation 2})$$

The function $\text{dist}_{\mathcal{B}}(u, v)$ computes the graph distance between points u and v ; i.e., the sum of the edge lengths along the path from u to v . The length $|\mathcal{B}_j|$ of edge j equals the Euclidean distance between the two endpoints of the edge.

What are the two architectures that minimize each objective (1) and (2) by itself? The optimal set of branches to minimize travel distance consists of the base connected directly to each leaf by a straight line (Figure 2B). We call this the Satellite tree. The optimal set of branches to minimize total length corresponds to the Steiner tree (Figure 2C). A Euclidean Steiner tree is a tree that connects all the input points whose total branch length is minimal, while allowing the addition of extra points that serve as branch points. Banavar et al. (2002) study metabolic scaling in source-directed transport networks and argue that the most efficient topology is one where the mean distance from the source (base) to the leaves is as small as possible; i.e., the tree is Satellite-like, although this solution has high network construction costs. On the other hand, Steiner-like trees minimize construction costs but are less mechanically stable (Niklas, 1999). These two solutions serve as anchors of the Pareto front, as we describe next.

Generating Solutions along the Pareto Front

There is tension between these two objectives: Satellite minimizes travel distance but has a large total length because each leaf is dedicated its own direct branch from the base. Steiner, on the other hand, minimizes total length but may have a large travel distance for some leaves. How well do plant architectures resolve this tension (Figure 2D)?

We hypothesize that if jointly minimizing total length and travel distance confers a selective fitness advantage for plant transport processes, then one might expect evolution to push plant architectures toward the Pareto front between these two objectives (Figure 3A) (Shoval et al., 2012). The concept of the Pareto front is often used to find the best compromise between competing objectives. In our case, the competing objectives are travel distance and total length. Consider two architectures, a_1 and a_2 . If a_2 has shorter length and shorter travel distance compared with a_1 (i.e., if a_2 “dominates” a_1), then natural selection will likely

eliminate a_1 from the population. Given sufficient genetic variation and sufficient evolutionary time, the theory posits that the only architectures that will remain in the population are those that lie on the Pareto front, as these architectures cannot be improved along both objectives at once. The precise location of an architecture on the front denotes specialization or a trade-off between the two objectives, which may vary across conditions and species depending on resource availability, and whichever confers the greatest fitness advantage in an environment. Since plants are among the most diverse species known and have been evolving for hundreds of millions of years (Hedges, 2002; Sussex and Kerk, 2001), it is natural to test this theory on plant architectures.

To generate solutions along the Pareto front that interpolate between Satellite and Steiner, we consider the simplest possible joint objective: a linear combination of the two individual objectives:

$$\begin{aligned} \text{Joint}(\mathcal{P}, \mathcal{B}) &= \min \alpha (\text{Length}) + (1 - \alpha) (\text{Travel}) \\ &= \min \alpha \left(\sum_j |\mathcal{B}_j| \right) + (1 - \alpha) \left(\sum_{i=1}^n \text{dist}_{\mathcal{B}}(\rho_0, \rho_i) \right), \end{aligned} \quad (\text{Equation 3})$$

where $0 \leq \alpha \leq 1$. If $\alpha = 0$, the optimal of the joint objective equals the Satellite. If $\alpha = 1$, the optimal equals the Steiner tree, and thus the joint optimization function is NP hard (Garey and Johnson, 1979). For $\alpha \in (0, 1)$, a wide variety of architectures can emerge that straddle the two anchors (Figures 2E–2G).

We developed a plant-inspired greedy algorithm to construct architectures that near-optimally minimize the joint objective for any given value of α (Algorithm S1). The algorithm initializes the network with a stem protruding from the base node and then iteratively connects leaves to the tree that minimally increases the value of the objective (STAR Methods).

Achieving Pareto Optimal Trade-Offs Guides Developmental Growth and Evolution

We scanned tomato plants daily over 20 days of development in ambient conditions (STAR Methods). On the first day of scanning (D0), there were only three points representing the base and the two cotyledons (embryonic leaves). By D20, there were 19 leaves and leaflets (Figure 1C), for which there is an enormous complexity of possible architectures: specifically, there are 5.48×10^{21} possible spanning trees on 19 points (Aigner and Ziegler, 2009), excluding Steiner nodes.

From each plant scan, we selected the 3D (x, y, z) locations corresponding to the base of the plant (ρ_0) and all the leaves and leaflets ($\rho_1, \rho_2, \dots, \rho_n$). Using these points, we calculated the Steiner optimal for total length, the Satellite optimal for travel distance, and the Pareto front using our greedy algorithm with

for $\alpha \in [0, 1]$. Inverted green triangles show a structurally stable architecture. Blue crosses represent 1,000 random architectures; panels with fewer (or altogether missing) crosses imply that these random architectures lay outside the plotting area, far away from the Pareto front, indicating that achieving Pareto optimality is unlikely by chance.

(E–G) In each panel, we show the distances to the Pareto front for the plant architectures (solid lines), stable architectures (dotted lines), and random architectures (dashed lines). In each panel, the x axis is the day of scanning, and the y axis is the log distance to the closest point on the Pareto front. Distances are normalized by the total length of the plant (mm) and are thus expressed as a percentage. Error bars indicate SEM over replicates. Overall, by comparing lines of the same color (condition) across architectures (plant, stable, random), we observe that plant architectures are much closer to the Pareto front than alternative architectures. Related to Figure S2 and Table S3.

different values of $\alpha \in (0, 1)$. These solutions all produce as output a tree. To compare these trees with the actual plant architecture (which is also a tree), we extracted the branch points from the scan and traced the skeletonized architecture that connected the base of the plant through the branch points to the leaves. All four solutions (Steiner, Satellite, the Pareto front, and the plant) were evaluated according to their travel distance and total length and were then plotted together in a trade-off diagram (Figure 3A). Each diagram in Figures 3B–3D only shows the Pareto analysis of a single plant scan taken on the final day of scanning; analysis of the full dataset of all 505 plant scans across species, conditions, and time points is shown in Figures 3E–3G (summarized in Table S3).

Strikingly, each tomato plant lay almost exactly on the Pareto front (Figure 3B) and this persisted over the entire 20 developmental days (Figure 3E). Overall, the average distance from the location of the plant to the Pareto front was only 0.36 mm (Figure S2A). This distance amounted to just 0.22% of the plant's total length (Table S3). This demonstrates that achieving well-balanced trade-offs may be an important growth strategy starting from very early in development and persisting through at least early maturation. It also suggests that the two proposed objectives capture important selective pressures that help dictate plant architecture.

Since plant architectures are highly plastic and influenced by many real-world factors, such as light availability, temperature, and nutrient status (Reinhardt and Kuhlemeier, 2002), we repeated the above experiment with tomato plants grown in four sub-optimal conditions: vegetational shade, high heat, high light, and drought (STAR Methods). As expected, there were many architectural changes in these conditions (Figure S1B). For example, consistent with the shade avoidance response (Casal, 2012), plant height was highest in shade (103.76 mm) versus other conditions (35.89 mm in drought, 38.13 mm in high heat, 43.33 mm in high light, and 63.93 mm in ambient; average D20). There were fewest leaves in high heat (5.3 ± 0.9) compared with drought (12.7 ± 1.2), shade (13.3 ± 0.9), ambient light (17.0 ± 0.8), and high light (20.7 ± 1.5). The total plant volume, measured by the convex hull of the plant's cloud points, varied across conditions by up to an order of magnitude: 13.78 cm³ in high heat, 135.21 cm³ in drought, 253.42 cm³ in shade, 598.84 cm³ in ambient, and 668.68 cm³ in high light. Thus, three important architectural features—plant height, number of leaves, and plant volume—showed significant plasticity across conditions.

Despite this diversity, plants grown in these four conditions still lay on or very close to the Pareto front (Figure 3B). Over all five conditions, the average distance from the plant to the Pareto front was 0.14% (high heat), 0.17% (shade), 0.22% (ambient), 0.48% (drought), and 3.17% (high light), with relatively little variation across replicates (Figure 3E and Table S3).

To test the significance of these results, we compared the actual plant architecture with two alternatives: random spanning trees and a structurally stable tree (Figures 2H and 2I; STAR Methods). Actual plant architectures all lay significantly closer to the Pareto front than these alternatives (Figure 3E and Table S3). For example, in ambient conditions, tomato plants were $0.22\% \pm 0.19\%$ from the Pareto front, compared with $34.44\% \pm 4.59\%$ for structural stability and $173.97\% \pm 17.81\%$

for random architectures ($p < 0.01\%$). This indicates that designing Pareto optimal architectures is not inevitable and an unlikely event by chance.

To further test the generality of this principle, we scanned two additional species (tobacco, which like tomato is a dicot, and sorghum, a monocot) through 20 days of development and across 3–4 conditions each (STAR Methods). We again observed a highly diverse range of architectures in these species across conditions (Figure S1B), but the architectures of both species still closely obeyed Pareto optimality (Figures 3C and 3D) and lay significantly closer to the Pareto front compared with the two alternatives (Figures 3F and 3G and Table S3). We also tested the theory on a wild-type, model plant (*Arabidopsis thaliana*) grown in greenhouse conditions and found similar behavior (Figure S3).

Overall, the architectures of 505 plants—scanned across multiple species (including monocots and dicots), growth conditions, and developmental time points—lay along or very close to the Pareto front, suggesting the generality of this principle.

Similarities and Differences in Trade-Off Strategies across Species and Conditions

The cost of building and maintaining infrastructure often influences the structure of biological networks. We measured cost as the total length of the plant used to connect the leaves to the root system. We found that all three plant species used architectures that achieved a large “bang for the buck”: compared with Satellite, plants reduced their total length by on average 54.6%, while only increasing travel distance by 6.5% (Table 1). In other words, a modest increase in travel distance provided a big savings in cost.

The location of the plant along the Pareto front can distinguish between species and conditions. To identify this location, we defined the trade-off ratio (STAR Methods) as the ratio of the excess length of the plant (compared with Steiner) to the excess travel distance of the plant (compared with Satellite). Larger trade-off ratios imply more emphasis on minimizing travel distance, thus being further to the right along the Pareto front (Figure 3A). Sorghum are grasses that visually have a more Satellite-like architecture, and indeed, their trade-off ratio was significantly larger than that of the two dicot species tested (average trade-off ratio of 1.312 for sorghum versus 1.149 for tomato and 1.099 for tobacco; $p < 0.01$ for both two-sample *t* tests). We also observed condition-specific differences. For example, in high heat, all three species produced architectures with the largest trade-off ratio compared with other conditions (Table 1), suggesting that high heat may bias plants toward architectures that make source-sink transport more efficient, at the expense of excess cost. In high light, the trade-off ratio was consistently the lowest (Table 1). Thus, the location of the plant along the Pareto front may represent systematic variation in growth strategies.

DISCUSSION

In this work, we generated a dataset of 505 above-ground plant architectures, collected across 3 species, grown in 3–5 environmental conditions for the same species, and through 20 development time points for the same plant. We derived a graph-theoretic algorithm to evaluate transport network design

Table 1. Variation in Trade-Off Strategies across Species and Conditions

Species	Condition	Length Reduction (%)	Travel Gain (%)	Trade-Off Ratio
Tomato	ambient	63.14 ± 0.63	6.68 ± 0.34	1.157 ± 0.02
Tomato	shade	68.20 ± 2.85	2.77 ± 0.09	1.129 ± 0.01
Tomato	high heat	48.47 ± 1.97	1.87 ± 0.19	1.328 ± 0.04
Tomato	drought	62.97 ± 1.14	5.43 ± 0.20	1.112 ± 0.01
Tomato	high light	61.93 ± 1.11	10.03 ± 0.41	1.020 ± 0.07
Tobacco	ambient	43.73 ± 1.03	12.47 ± 1.03	0.969 ± 0.01
Tobacco	shade	52.53 ± 0.74	8.07 ± 0.68	1.130 ± 0.04
Tobacco	high heat	47.05 ± 3.95	10.15 ± 0.35	1.198 ± 0.00
Sorghum	ambient	49.97 ± 0.70	4.67 ± 0.12	1.373 ± 0.04
Sorghum	shade	53.70 ± 0.17	4.00 ± 0.36	1.234 ± 0.05
Sorghum	high heat	57.20 ± 0.45	4.13 ± 0.12	1.460 ± 0.04
Sorghum	high light	46.33 ± 0.35	7.73 ± 0.37	1.181 ± 0.04
		Average: 54.60	Average: 6.50	

The average (±SE) total length reduction, travel distance gain, and trade-off ratio for each species and condition. See [STAR Methods](#) for definitions. Related to [Table S1](#).

trade-offs, and we showed that plant architectures are Pareto optimal with respect to a simple performance and cost trade-off. Prior studies to our knowledge have not studied how well such trade-offs are resolved when building networks to connect points in 3D space, where the only assumed input is the locations of the base and leaves, and the desired output is a network connecting the points. We also showed species- and condition-specific differences in where the plants lay on the Pareto front, suggesting that variants on the same fundamental network design trade-off may guide plant structure across species and conditions. Finally, architectures remained near the Pareto front through 20 days of measurements, suggesting that these trade-offs influence growth strategies starting from very early in development.

Although general, the two measures we study (total length and travel distance) relate to several known biological factors that affect the performance of plant architectures. By focusing only on lengths, we made a clear and testable theoretical prediction (Pareto optimality), without requiring a model with many parameters. There are, however, numerous other features that also affect the performance of plant architectures that we did not consider here. For example, travel distance (related to hydraulic resistance) depends on both the lengths and the radii of branches when considering Poiseuille flow (radius⁴ versus 1/length); similarly, a more accurate measure of construction costs (total length) would relate to the surface area as radius². The radii of branches are not uniform across the architecture and can be regulated by condition; for example, for tomato plants grown in high light, we observed a 61% increase in stem diameter compared with plants grown in ambient light on day 20 (4.314 mm versus 2.681 mm). Prior work has derived some constraints on branch radii, for example, Leonardo's rule (Eloy, 2011) as well as other allometries (Bentley et al., 2013). Beyond radii, there are also other important features to model, including light interception, mechanical stress, and leaf size (Niklas, 1999; Puijalón et al., 2011). Thus, while lengths are clearly important, we do not suggest that they alone capture the full complexity of plant architectures. Further, our graph-theoretic

algorithm is not intended to represent an alternative model of plant branching, which has been the focus of decades of prior work (see [Introduction](#)); however, our observation of Pareto optimality may provide a new constraint for these models.

Our focus on evaluating architectures according to two general network design principles was also motivated by their similar role in optimizing branching morphologies in other biological networks. For example, in neurons, action potentials produced at the soma must be transported to post-synaptic neurons via a branching axonal arbor. Consider the soma of the neuron as analogous to the base of the plant and the post-synaptic partners as leaves; travel distance, then, is equivalent to Cajal's law of conduction delay (Budd et al., 2010), which states that axonal branching attempts to minimize the time required to propagate an action potential from the soma to its post-synaptic partners (Cuntz et al., 2010). Total length is a measure of wiring economy, which states that neurons also try to minimize the total amount of wire required to make its desired connections. Both objectives have been shown to constrain circuit wiring in many brain regions and species (Rivera-Alba et al., 2014). Trade-offs between these two properties also influence the design of cardiovascular networks (Tekin et al., 2016; Hunt and Savage, 2016) and leaf venation networks (Ronellenfitsch and Katifori, 2016), where the requirement for robustness has been shown to produce loops or cycles (Katifori et al., 2010). Thus, despite the many mechanistic differences across engineered and biological systems, this suggests that there may be universal optimization principles shared by both (Baluška et al., 2006; Navlakha and Bar-Joseph, 2011).

The insights derived here may also raise new challenges for experimental plant biologists. For example, our observation that plant architectures are Pareto optimal raises immediate questions about the molecular and cellular mechanisms responsible for implementing this trade-off. Different structural patterns across conditions for the same species may be generated by up- or downregulation of a few core genes (Abzhanov et al., 2004; Abzhanov et al., 2006; Stevens, 2009). The trade-offs quantified here may also reveal new selection strategies for plant breeding

that are vital for increasing food supply in a changing climate and increasing human population; it may also inform network construction problems in other domains (e.g., electric grids).

Finally, are there exceptions to the network design principles studied here? While most of the plants fell on or close to the Pareto front, we did find some deviation for plants grown in the high-light condition. Excessive light can be stressful to plants (Barber and Andersson, 1992); the deviation we observed suggests that plant architectures in this condition may also optimize other objectives in addition to travel distance and total length. Recent advances in Pareto analysis may be useful in this case to infer additional candidate objectives given architecture traits (Hart et al., 2015). Further, we studied four plant species across multiple conditions; these species are not meant to represent the entire plant kingdom, nor are these conditions representative of every possible growth climate for plants. As more 3D architectures are mapped across different environments and longer time-scales, it would be important to further test the generality of this trade-off principle.

STAR★METHODS

Detailed methods are provided in the online version of this paper and include the following:

- KEY RESOURCES TABLE
- CONTACT FOR RESOURCE SHARING
- EXPERIMENTAL MODEL AND SUBJECT DETAILS
 - Plant Growth Experiments
- METHOD DETAILS
 - Plant 3D Scanning
 - Selection of Input Points
- QUANTIFICATION AND STATISTICAL ANALYSIS
 - Quantifying Total Length Reduction, Travel Distance Gain, and Trade-off Ratio
 - Algorithm to Generate Solutions on the Pareto Front
 - Comparison to Structurally Stable Architectures and Random Architectures
 - The Relationship of Pareto Optimality with Other Optimization Approaches
- DATA AND SOFTWARE AVAILABILITY

SUPPLEMENTAL INFORMATION

Supplemental Information includes three figures, three tables, and one algorithm and can be found with this article online at <http://dx.doi.org/10.1016/j.cels.2017.06.017>.

AUTHOR CONTRIBUTIONS

A.C., U.V.P., J.C., and S.N. conceived the study. A.C., U.V.P., and S.N. performed the experiments. S.N. analyzed the data. A.C., U.V.P., J.C., and S.N. wrote the paper.

ACKNOWLEDGMENTS

J.C. is an Investigator for the Howard Hughes Medical Institute (HHMI). The authors thank HHMI for purchasing the 3D scanning equipment; the Salk Innovation Grant for funding support; and Charles F. Stevens and David Peterson for useful discussions. S.N. thanks the Army Research Office (grant DOD W911NF-17-1-0045) for funding support.

Received: November 28, 2016

Revised: March 15, 2017

Accepted: June 29, 2017

Published: July 26, 2017

REFERENCES

- Abzhanov, A., Protas, M., Grant, B.R., Grant, P.R., and Tabin, C.J. (2004). Bmp4 and morphological variation of beaks in Darwin's finches. *Science* 305, 1462–1465.
- Abzhanov, A., Kuo, W.P., Hartmann, C., Grant, B.R., Grant, P.R., and Tabin, C.J. (2006). The calmodulin pathway and evolution of elongated beak morphology in Darwin's finches. *Nature* 442, 563–567.
- Aigner, M., and Ziegler, G.M. (2009). *Proofs from THE BOOK*, Fourth Edition (Springer).
- Allen, M.T., Prusinkiewicz, P., and DeJong, T.M. (2005). Using L-systems for modeling source-sink interactions, architecture and physiology of growing trees: the L-PEACH model. *New Phytol.* 166, 869–880.
- Baluška, F., Mancuso, S., and Volkman, D. (2006). *Communication in Plants: Neuronal Aspects of Plant Life* (Springer).
- Banavar, J.R., Damuth, J., Maritan, A., and Rinaldo, A. (2002). Supply-demand balance and metabolic scaling. *Proc. Natl. Acad. Sci. USA* 99, 10506–10509.
- Barber, J., and Andersson, B. (1992). Too much of a good thing: light can be bad for photosynthesis. *Trends Biochem. Sci.* 17, 61–66.
- Bentley, L.P., Stegen, J.C., Savage, V.M., Smith, D.D., von Allmen, E.I., Sperry, J.S., Reich, P.B., and Enquist, B.J. (2013). An empirical assessment of tree branching networks and implications for plant allometric scaling models. *Ecol. Lett.* 16, 1069–1078.
- Bloom, A.J., Chapin, F.S., and Mooney, H.A. (1985). Resource limitation in plants—an economic analogy. *Annu. Rev. Ecol. Syst.* 16, 363–392.
- Boudon, F., Pradal, C., Cokelaer, T., Prusinkiewicz, P., and Godin, C. (2012). L-py: an L-system simulation framework for modeling plant architecture development based on a dynamic language. *Front. Plant Sci.* 3, 76.
- Budd, J.M., Kovacs, K., Ferecsko, A.S., Buzas, P., Eysel, U.T., and Kisvarday, Z.F. (2010). Neocortical axon arbors trade-off material and conduction delay conservation. *PLoS Comput. Biol.* 6, e1000711.
- Cabanes, G., van Wilgenburg, E., Beekman, M., and Latty, T. (2014). Ants build transportation networks that optimize cost and efficiency at the expense of robustness. *Behav. Ecol.* 26, 223–231.
- Casal, J.J. (2012). Shade avoidance. *The Arabidopsis Book* 10, e0157.
- Chitwood, D.H., Headland, L.R., Filiault, D.L., Kumar, R., Jimenez-Gomez, J.M., Schragar, A.V., Park, D.S., Peng, J., Sinha, N.R., and Maloof, J.N. (2012). Native environment modulates leaf size and response to simulated foliar shade across wild tomato species. *PLoS One* 7, e29570.
- Chitwood, D.H., Kumar, R., Ranjan, A., Pelletier, J.M., Townsley, B.T., Ichihashi, Y., Martinez, C.C., Zumstein, K., Harada, J.J., Maloof, J.N., and Sinha, N.R. (2015). Light-Induced indeterminacy alters shade-avoiding tomato leaf morphology. *Plant Physiol.* 169, 2030–2047.
- Chitwood, D.H., Rundell, S.M., Li, D.Y., Woodford, Q.L., Yu, T.T., Lopez, J.R., Greenblatt, D., Kang, J., and Londo, J.P. (2016). Climate and developmental plasticity: interannual variability in grapevine leaf morphology. *Plant Physiol.* 170, 1480–1491.
- Corson, F. (2010). Fluctuations and redundancy in optimal transport networks. *Phys. Rev. Lett.* 104, 048703.
- Cuntz, H., Forstner, F., Borst, A., and Hausser, M. (2010). One rule to grow them all: a general theory of neuronal branching and its practical application. *PLoS Comput. Biol.* 6, e1000877.
- Domec, J.C., Lachenbruch, B., Meinzer, F.C., Woodruff, D.R., Warren, J.M., and McCulloh, K.A. (2008). Maximum height in a conifer is associated with conflicting requirements for xylem design. *Proc. Natl. Acad. Sci. USA* 105, 12069–12074.
- Eloy, C. (2011). Leonardo's rule, self-similarity, and wind-induced stresses in trees. *Phys. Rev. Lett.* 107, 258101.

- Farnsworth, K.D., and Niklas, K.J. (1995). Theories of optimization, form and function in branching architecture in plants. *Funct. Ecol.* **9**, 355–363.
- Fonseca, R., Brazil, M., Winter, P., and Zachariasen, M. (2014). Faster exact algorithm for computing Steiner trees in higher dimensional Euclidean spaces. *Proceedings of the 11th DIMACS Implementation Challenge Workshop*.
- Fourcaud, T., Zhang, X., Stokes, A., Lambers, H., and Korner, C. (2008). Plant growth modelling and applications: the increasing importance of plant architecture in growth models. *Ann. Bot.* **101**, 1053–1063.
- Garey, M.R., and Johnson, D.S. (1979). *Computers and Intractability: A Guide to the Theory of NP-Completeness* (W.H. Freeman).
- Godin, C. (2000). Representing and encoding plant architecture: a review. *Ann. For. Sci.* **57**, 413–438.
- Godin, C., and Ferraro, P. (2010). Quantifying the degree of self-nestedness of trees: application to the structural analysis of plants. *IEEE/ACM Trans. Comput. Biol. Bioinform.* **7**, 688–703.
- Guo, Y., Fourcaud, T., Jaeger, M., Zhang, X., and Li, B. (2011). Plant growth and architectural modelling and its applications. Preface. *Ann. Bot.* **107**, 723–727.
- Hart, Y., Sheftel, H., Hausser, J., Szekely, P., Ben-Moshe, N.B., Korem, Y., Tendler, A., Mayo, A.E., and Alon, U. (2015). Inferring biological tasks using Pareto analysis of high-dimensional data. *Nat. Methods* **12**, 233–235.
- Heckwolf, S., Heckwolf, M., Kaeppeler, S.M., de Leon, N., and Spalding, E.P. (2015). Image analysis of anatomical traits in stalk transections of maize and other grasses. *Plant Methods* **11**, 26.
- Hedges, S.B. (2002). The origin and evolution of model organisms. *Nat. Rev. Genet.* **3**, 838–849.
- Hunt, D., and Savage, V.M. (2016). Asymmetries arising from the space-filling nature of vascular networks. *Phys. Rev. E* **93**, 062305.
- Jean, R. (2009). *Phyllotaxis: A Systemic Study in Plant Morphogenesis* (Cambridge University Press).
- Katifori, E., Szollosi, G.J., and Magnasco, M.O. (2010). Damage and fluctuations induce loops in optimal transport networks. *Phys. Rev. Lett.* **104**, 048704.
- Kennedy, M.C. (2010). Functional–structural models optimize the placement of foliage units for multiple whole-canopy functions. *Ecol. Res.* **25**, 723–732.
- Kim, Y., Sinclair, R., Chindapol, N., Kaandorp, J.A., and De Schutter, E. (2012). Geometric theory predicts bifurcations in minimal wiring cost trees in biology are flat. *PLoS Comput. Biol.* **8**, e1002474.
- Leon, J., Rojo, E., and Sanchez-Serrano, J.J. (2001). Wound signalling in plants. *J. Exp. Bot.* **52**, 1–9.
- Mandelbrot, B., and Novak, M. (2004). *Thinking in Patterns: Fractals and Related Phenomena in Nature* (World Scientific).
- McCulloh, K.A., Sperry, J.S., and Adler, F.R. (2003). Water transport in plants obeys Murray's law. *Nature* **427**, 939–942.
- Murphy, R.L., Klein, R.R., Morishige, D.T., Brady, J.A., Rooney, W.L., Miller, F.R., Dugas, D.V., Klein, P.E., and Mullet, J.E. (2011). Coincident light and clock regulation of pseudoreponse regulator protein 37 (PRR37) controls photoperiodic flowering in sorghum. *Proc. Natl. Acad. Sci. USA* **108**, 16469–16474.
- Navlakha, S., and Bar-Joseph, Z. (2011). Algorithms in nature: the convergence of systems biology and computational thinking. *Mol. Syst. Biol.* **7**, 546.
- Newman, M. (2010). *Networks: An Introduction* (Oxford University Press).
- Nguyen, T.T., Slaughter, D.C., Max, N., Maloof, J.N., and Sinha, N. (2015). Structured light-based 3D reconstruction system for plants. *Sensors (Basel)* **15**, 18587–18612.
- Niklas, K.J. (1999). Evolutionary walks through a land plant morphospace. *J. Exp. Bot.* **50**, 39–52.
- Niklas, K.J. (2004). Plant allometry: is there a grand unifying theory? *Biol. Rev. Camb. Philos. Soc.* **79**, 871–889.
- Ochoa, G. (1998). Genetic Algorithms and Lindenmayer Systems. In *Proc. 5th Intl. Conf. on Parallel Problem Solving from Nature*, A.E. Eiben, Th. Bäck, M. Schoenauer, and H.-P. Schwefel, eds. (Springer), pp. 335–344.
- Peel, A. (2013). *Transport of Nutrients in Plants* (Elsevier Science).
- Pestana, S.G., Rijpkema, E., Radulescu, A., Goossens, K., and Gangwal, O.P. (2004). Cost-performance trade-offs in networks on chip: a simulation-based approach. In *Design, Automation and Test in Europe Conference and Exhibition, 2004. Proceedings, Volume 2 (IEEE)*, pp. 764–769.
- Price, C.A., and Weitz, J.S. (2012). Allometric covariation: a hallmark behavior of plants and leaves. *New Phytol.* **193**, 882–889.
- Price, C.A., Enquist, B.J., and Savage, V.M. (2007). A general model for allometric covariation in botanical form and function. *Proc. Natl. Acad. Sci. USA* **104**, 13204–13209.
- Price, C.A., Ogle, K., White, E.P., and Weitz, J.S. (2009). Evaluating scaling models in biology using hierarchical Bayesian approaches. *Ecol. Lett.* **12**, 641–651.
- Price, C.A., Gilooly, J.F., Allen, A.P., Weitz, J.S., and Niklas, K.J. (2010). The metabolic theory of ecology: prospects and challenges for plant biology. *New Phytol.* **188**, 696–710.
- Prusinkiewicz, P., and Lindenmayer, A. (1996). *The Algorithmic Beauty of Plants* (Springer-Verlag).
- Prusinkiewicz, P., and Runions, A. (2012). Computational models of plant development and form. *New Phytol.* **193**, 549–569.
- Puijalon, S., Bouma, T.J., Douady, C.J., van Groenendael, J., Anten, N.P., Martel, E., and Bornette, G. (2011). Plant resistance to mechanical stress: evidence of an avoidance-tolerance trade-off. *New Phytol.* **191**, 1141–1149.
- Reinhardt, D., and Kuhlemeier, C. (2002). Plant architecture. *EMBO Rep.* **3**, 846–851.
- Rivera-Alba, M., Peng, H., de Polavieja, G.G., and Chklovskii, D.B. (2014). Wiring economy can account for cell body placement across species and brain areas. *Curr. Biol.* **24**, R109–R110.
- Roitsch, T. (1999). Source-sink regulation by sugar and stress. *Curr. Opin. Plant Biol.* **2**, 198–206.
- Rolland, F., Moore, B., and Sheen, J. (2002). Sugar sensing and signaling in plants. *Plant Cell* **14 (Suppl 1)**, S185–S205.
- Ronellenfitsch, H., and Katifori, E. (2016). Global optimization, local adaptation, and the role of growth in distribution networks. *Phys. Rev. Lett.* **117**, 138301.
- Savage, V.M., Bentley, L.P., Enquist, B.J., Sperry, J.S., Smith, D.D., Reich, P.B., and von Allmen, E.I. (2010). Hydraulic trade-offs and space filling enable better predictions of vascular structure and function in plants. *Proc. Natl. Acad. Sci. USA* **107**, 22722–22727.
- Shinozaki, K., YODA, K., Hozumi, K., and Kira, T. (1964). A quantitative analysis of plant form; the pipe model theory. I. *Jpn. J. Ecol.* **14**, 97–105.
- Shoval, O., Sheftel, H., Shinar, G., Hart, Y., Ramote, O., Mayo, A., Dekel, E., Kavanagh, K., and Alon, U. (2012). Evolutionary trade-offs, Pareto optimality, and the geometry of phenotype space. *Science* **336**, 1157–1160.
- Simini, F., Anfodillo, T., Carrer, M., Banavar, J.R., and Maritan, A. (2010). Self-similarity and scaling in forest communities. *Proc. Natl. Acad. Sci. USA* **107**, 7658–7662.
- Smith, W.D. (1992). How to find Steiner minimal trees in euclidean-space. *Algorithmica* **7**, 137–177.
- Smith, D.D., Sperry, J.S., Enquist, B.J., Savage, V.M., McCulloh, K.A., and Bentley, L.P. (2014). Deviation from symmetrically self-similar branching in trees predicts altered hydraulics, mechanics, light interception and metabolic scaling. *New Phytol.* **201**, 217–229.
- Sperry, J.S., Smith, D.D., Savage, V.M., Enquist, B.J., McCulloh, K.A., Reich, P.B., Bentley, L.P., and von Allmen, E.I. (2012). A species-level model for metabolic scaling in trees I. Exploring boundaries to scaling space within and across species. *Funct. Ecol.* **26**, 1054–1065.
- Stevens, C.F. (2009). Darwin and Huxley revisited: the origin of allometry. *J. Biol.* **8**, 14.
- Sussex, I.M., and Kerk, N.M. (2001). The evolution of plant architecture. *Curr. Opin. Plant Biol.* **4**, 33–37.
- Szekely, P., Korem, Y., Moran, U., Mayo, A., and Alon, U. (2015). The mass-lengthy triangle: Pareto optimality and the geometry of life-history trait space. *PLoS Comput. Biol.* **11**, e1004524.

- Tekin, E., Hunt, D., Newberry, M.G., and Savage, V.M. (2016). Do vascular networks branch optimally or randomly across spatial scales? *PLoS Comput. Biol.* *12*, e1005223.
- Tendler, A., Mayo, A., and Alon, U. (2015). Evolutionary tradeoffs, Pareto optimality and the morphology of ammonite shells. *BMC Syst. Biol.* *9*, 12.
- Tero, A., Takagi, S., Saigusa, T., Ito, K., Bebber, D.P., Fricker, M.D., Yumiki, K., Kobayashi, R., and Nakagaki, T. (2010). Rules for biologically inspired adaptive network design. *Science* *327*, 439–442.
- Vos, J., Evers, J.B., Buck-Sorlin, G.H., Andrieu, B., Chelle, M., and de Visser, P.H. (2010). Functional-structural plant modelling: a new versatile tool in crop science. *J. Exp. Bot.* *61*, 2101–2115.
- West, G.B., Brown, J.H., and Enquist, B.J. (1999). The fourth dimension of life: fractal geometry and allometric scaling of organisms. *Science* *284*, 1677–1679.
- Williams, L.E., Lemoine, R., and Sauer, N. (2000). Sugar transporters in higher plants—a diversity of roles and complex regulation. *Trends Plant Sci.* *5*, 283–290.

STAR★METHODS

KEY RESOURCES TABLE

REAGENT or RESOURCE	SOURCE	IDENTIFIER
Deposited Data		
Plant 3D architecture data		plant3d.sn1.salk.edu
Plant 3D architecture data		http://dx.doi.org/10.17632/9k7zctdyhs.1
Experimental Models: Organisms/Strains		
Tomato (<i>Solanum lycopersicum cv m82D</i>)	Plant Biology Laboratories, Salk Institute	
Tobacco (<i>Nicotiana benthamiana</i>)	Plant Biology Laboratories, Salk Institute	
Sorghum (<i>Sorghum bicolor, 100m</i>)	John Mullet, Texas A&M University	
Software and Algorithms		
Code to compute Pareto optimality test	This paper	plant3d.sn1.salk.edu
3D scanner (Faro Technologies)		http://www.faro.com/products/metrology/faroarm-measuring-arm/overview
Other		
Plant growth chambers	Percival Scientific, IA	https://www.percival-scientific.com/
Plant growth chambers	Conviron model E8	http://www.conviron.com/products/e8-reach-in-plant-growth-chamber

CONTACT FOR RESOURCE SHARING

Further information and requests for resources should be directed to and will be fulfilled by the Lead Contact, Saket Navlakha (navlakha@salk.edu).

EXPERIMENTAL MODEL AND SUBJECT DETAILS

Plant Growth Experiments

Scanning was performed on three species of plants (Table S1): tomato (*Solanum lycopersicum cv m82D*), tobacco (*Nicotiana benthamiana*), and sorghum (*Sorghum bicolor 100m* [Murphy et al., 2011]). Plants were grown in a medium comprised of 2x soil (SunGro Propagation mix, USA) to 1x medium vermiculite (SunGro, USA) and was moistened with water containing 0.12–0.24 oz/gallon fertilizer (Plantex, Canada). Tomato and tobacco seedlings were planted in 12-celled planting trays and then transferred to plastic pots. Tomatoes were transferred to 4in. diameter x 3in. tall plastic pots on day 9 after planting, and were first scanned on day 11 after planting (which we call scanning day 0, or D0). Tobaccos were transferred to 4.5in. diameter x 3.75in. tall plastic pots on day 9 after planting, and were first scanned on day 17. Sorghum were directly planted in 4in. diameter x 3in. tall plastic pots, and were first scanned on day 7. Plants were provided approximately 50mL of water per day while in the greenhouse; roughly 24 hours prior to scanning day 0, plants were moved from the greenhouse into their environmental growth condition.

For each species, experiments were performed across 3–5 environmental test conditions in laboratory growth chambers (Table S1). Plants were grown on a long-day cycle with 8hr dark (1am–9am) and 16hr light (9am–1am). Plants received 50mL of water every alternate day, with the exception of the drought condition, where no water was provided after scanning day 0. Tomato experiments were performed in 5 conditions: ambient light (Percival Scientific, IA; 22°C), shade (22°C, R:FR=0.7), high-heat (35°C), high-light (Conviron model E8; 22°C, PAR=1140 $\mu\text{mol}^{-2}\text{m}^{-1}$), and drought (22°C). Tobacco experiments were performed in 3 conditions: ambient light, shade, and high-heat (32°C). Sorghum experiments were performed in 4 conditions: ambient light, shade, high-heat (35°C), and high-light.

Each plant was scanned every 1–2 days through roughly 20 days of development (D20–D22). For each species-condition combination, 2–5 replicates were used. Scans were performed at approximately the same time every scanning day.

The plant species studied were selected because of their broad agricultural importance, and because they represent two well-known classes of plant architectures (monocots and dicots). The conditions selected represent a broad range of environmental conditions that many plants must prevail through to survive.

METHOD DETAILS

Plant 3D Scanning

A high-resolution blue-laser scanner (Edge Scan Arm HD, Faro Inc.) was used to generate a 3D point cloud representation of each scanned plant. Spatial encoders in the arm provide automatic registration in 3D space, avoiding issues in imaging-based approaches that require additional segmentation and alignment in the analysis [Nguyen et al., 2015, Heckwolf et al., 2015]. Each plant was scanned from two opposite sides and then automatically aligned. Computation of the distance from the plant architecture to the Pareto front was on the order of millimeters, whereas the scanner provides micron-level resolution with an error ± 25 μm ; thus, we do not believe error in scanning precision affect our conclusions. The number of cloud points for younger plants was on the order of tens of thousands; elder, more mature plants had up to 1 million cloud points. Accompanying software (Polyworks 2016, USA) was used to generate a triangulation mesh of the point cloud.

Selection of Input Points

Using Polyworks, points were selected corresponding to the base of the stem, all leaves and leaflets, and all branch points on the hypocotyl, stem, and petioles (used for tracing the skeleton architecture). For tomatoes, leaf points were chosen at the base of each leaflet. Although tomato plants may have a similar general structure for compound leaves, we treated each leaflet separately because we found branch angles and petiole lengths to be highly plastic across species, conditions, and time [Chitwood et al., 2012, Chitwood et al., 2015, 2016]; this also allowed us to test whether tree structures with higher branch orders (composed of several individual leaf structures) were Pareto optimal. Tobacco leaves have only one leaf per petiole, and hence leaf points were chosen at the base of each leaf. Sorghum do not have petioles and instead have long grassy leaves; hence leaf points were selected at two locations per leaf: the highest point of the leaf in the up-down (y) direction, and the half-way point between the base of the leaf (where the leaf branches from the stalk) and the highest point. For sorghums grown in high light, multiple stalk split from the base of the stem in later days, and only the middle structure was considered for computational efficiency.

QUANTIFICATION AND STATISTICAL ANALYSIS

The data were quantified using the graph-theoretic features of travel distance and total length. We used $n = 505$ architectures. To determine the likelihood that a plant architecture would lie on the Pareto front, we compared the plant's distance to the Pareto front versus two baseline architectures: random spanning trees and a structurally stable tree. These and other technical details are described in Results, Figure Legends, and Methods.

Quantifying Total Length Reduction, Travel Distance Gain, and Trade-off Ratio

The following quantities compare the travel distance and total length of the plant versus the Satellite:

$$\text{Length Reduction} : = \frac{|\text{Length}_{\text{plant}} - \text{Length}_{\text{satellite}}|}{\text{Length}_{\text{satellite}}} \quad (\text{Equation 4})$$

$$\text{Travel Gain} : = \frac{\text{Travel}_{\text{plant}} - \text{Travel}_{\text{satellite}}}{\text{Travel}_{\text{satellite}}} \quad (\text{Equation 5})$$

The former measures the difference in total length as a percentage of the Satellite length. Because the plant length is always shorter than the Satellite length, the absolute value is taken. The latter measures the gain in travel distance as a percentage of the Satellite travel distance.

The following quantity measures how the plant trades-off total length and travel distance with respect to the corresponding optimals:

$$\text{Trade - off Ratio} : = \frac{\text{Length}_{\text{plant}}/\text{Length}_{\text{steiner}}}{\text{Travel}_{\text{plant}}/\text{Travel}_{\text{satellite}}}, \quad (\text{Equation 6})$$

The numerator measures the fold increase in length used by the plant compared to the Steiner optimal. The denominator measures the fold increase in travel distance required by the plant compared to the Satellite optimal. A plant with a high trade-off ratio (i.e. large numerator, small denominator) implies that it emphasizes optimizing travel distance. A plant with a low trade-off value (i.e. small numerator, large denominator) implies that it emphasizes optimizing total length.

Algorithm to Generate Solutions on the Pareto Front

First, we describe how we generated the two anchors of the Pareto front. Computing the Satellite optimal is trivial for any given input. Computing the optimal Steiner tree for a set of points in 3D Euclidean space is a classic NP-hard problem [Garey and Johnson, 1979].

However, because most of our plants generate <20 leaves during the time-frame we study, we were able to compute the optimal Steiner tree using exact solvers [Smith, 1992, Fonseca et al., 2014] in a reasonable amount of time (up to 2–3 days for the largest plants).

To generate architectures that interpolate between these two anchors, we developed a plant-inspired greedy algorithm. The algorithm initializes the tree with the base node p_0 and a stem that connects the base to the centroid of the n leaves. Along the stem, we add evenly spaced Steiner nodes, which are non-input nodes from which future branches can connect. The stem also provides structural stability to support the plant's growth. In each step of the algorithm, an edge is added between an unconnected leaf node u and some existing node v (including Steiner nodes) in the tree. We add the edge to the tree that minimally increases the value of the objective. Steiner nodes are also included along every edge added. The algorithm terminates when all n leaf nodes have been added to the tree. Pseudocode for the algorithm is shown in Algorithm S1.

To generate the Pareto front, we varied $\alpha \in [0, 1]$ in step sizes of 0.01. As α varies, different architectures emerge (Figures 2E–2G).

Cuntz et al. developed an algorithm to generate spanning trees to connect input points inspired by similar objectives in neural branching morphologies [Cuntz et al., 2010]. In their work, travel distance corresponds to a path length cost between the cell body and the neuron's synaptic contact points; total length corresponds to a wiring cost. There are two differences between our algorithm and Cuntz et al.: First, we initialize our tree with a stem emanating from the base. Second, every edge we add (including the stem) includes Steiner points that can be used as branch points. Cuntz et al. only produce a spanning tree with no Steiner points: they initialize their algorithm with an empty tree with only the base node, and in each step an edge is added — either between the base and a leaf node or between two leaf nodes — that minimize the objective. The addition of the stem and Steiner nodes in our algorithm helps reduce the value of the objective for 76% of the plants (Table S2, left). In our work, we did not assume any given assignment of leaves to hierarchical levels in the tree [Savage et al., 2010], though this is because we only consider lengths; if branch radii information were included, some hierarchical labeling may also be needed.

As mentioned above, we were able to compute the optimal Steiner tree using exact solvers with running time on the order of 2–3 days for most of the largest plants. While our joint objective may also be amenable to exact optimization, exact Steiner tree solvers reduce the search space using assumptions that are highly-tuned to the pure Steiner tree problem, and that we were not able to modify to account for the joint objective. However, we did compare the quality of the solution generated by our algorithm for $\alpha = 1$ to the optimal Steiner tree (Table S2, right). Overall, the value of the joint objective for our algorithm was on average only 5.97% higher than the Steiner tree. As α decreases, this difference decreases since our algorithm converges to the Satellite optimal for $\alpha = 0$. Thus, the Pareto front produced by our algorithm is very close to optimal.

Comparison to Structurally Stable Architectures and Random Architectures

We compared the actual plant architectures with two alternative architectures to show that achieving Pareto-optimality is not trivial nor likely to happen by chance.

The first alternative was random architectures, where points $P = (p_0, p_1, \dots, p_n)$ were connected by a random spanning tree. This spanning tree was constructed by first popping a random point v_0 from P and adding it to the tree. We then popped another random (unconnected) point from P and connected it to a random point that was already added to the tree. We repeated this process until all points were added to the tree. This random spanning tree construction process was repeated 1000 times to create 1000 random spanning trees.

The second alternative was a structurally stable architecture. This was created by forming a vertical stem connecting the base node to the centroid of the n leaves, and then connecting each leaf to this centroid point via a straight line, which provides even weight dispersion.

The Relationship of Pareto Optimality with Other Optimization Approaches

The method of Pareto optimality represents a type of multi-dimension optimization that uses a single parameter (α) to balance the trade-off between two objectives. Another formulation of our problem might have been to minimize travel distance subject to a constraint on total length. Then, by introducing a variable (λ , commonly called the Lagrangian multiplier), we can move the constraint into the optimization itself, which gives rise to a Lagrangian function. Our greedy algorithm for generating the Pareto front could then be similarly used to optimize the Lagrangian function and determine closeness to optimality for the plants. Thus, there is a close resemblance between the method of Pareto optimality and that of Lagrangian optimization. The Pareto optimality method also generates a type of 2D fitness landscape, where the global maxima of the landscape corresponds to any location on the Pareto front where an optimal compromise between the two objectives is achieved; selective pressure is then assumed to push architectures towards this front. The method of Pareto optimality has been used in numerous studies in biology before [Shoval et al., 2012, Szekely et al., 2015, Tendler et al., 2015], lending precedence to their use here.

DATA AND SOFTWARE AVAILABILITY

Data for the 505 3D plant architectures are available to download at Mendeley Data (<http://dx.doi.org/10.17632/9k7zctdyhs.1>). Code for computing the Pareto front analysis, and visualizations of all plant architectures, are available at: <http://plant3d.sn1.salk.edu>.